Field-Reversed Configurations in an Unmagnetized Plasma

R. L. Stenzel,* J. M. Urrutia, and K. D. Strohmaier

Department of Physics and Astronomy, University of California, Los Angeles, California 90095-1547, USA

(Received 12 June 2008; published 24 September 2008)

An oscillating magnetic field is applied with a loop antenna to an unmagnetized plasma. At small amplitudes the field is evanescent. At large amplitudes the field magnetizes the electrons, which allows deeper field penetration in the whistler modes. Field-reversed configurations are formed at each half cycle. Electrons are energized. Transient whistler instabilities produce high-frequency oscillations in the magnetized plasma volume.

DOI: 10.1103/PhysRevLett.101.135002 PACS numbers: 52.35.Hr, 52.35.Mw, 52.55.Lf, 94.05.Rx

The penetration of a time-dependent magnetic field into unmagnetized plasma is a problem of broad interest in areas such as inductively coupled plasmas [1], plasma opening switches [2], and very low frequency magnetic loop antennas [3]. Well known are the classical skin depth $\delta = (2/\mu_0\omega\sigma)^{1/2}$ in collisional plasmas of conductivity $\sigma \gg \omega\epsilon_0$ and the collisionless skin depth c/ω_p in cold collisionless plasma of plasma frequency $\omega_p \gg \omega$ [4]. In hot collisionless plasmas, an anomalous skin effect arises from the electron transit time through the skin layer [5–7]. Nonlinear effects can change the penetration depth due to modifications of the density [8], conductivity [9], and the Lorentz force of the rf magnetic field [10]. In the high-field limit, the electrons become fully magnetized and the field can penetrate as a nonlinear electron magnetohydrodynamic wave into the plasma [2,11,12].

We show in the present Letter that a strong oscillatory magnetic field applied to an unmagnetized plasma magnetizes electrons, which allows the field to penetrate in the whistler mode over a distance larger than the skin depth. The field embedded by one half cycle is still present when the next half cycle starts, leading to the formation of field-reversed configurations (FRCs) with toroidal null lines and radial three-dimensional (3D) null points. It is worth noting that FRCs have been studied extensively for their fusion potential [13]. Field penetration into the plasma produces an elongation of the FRC in the axial direction. Magnetic helicity forms at the expanding fronts. The sign of the helicity is consistent with that of whistlers. High-frequency magnetic oscillations are observed for large fields, indicating a possible whistler instability in the toroidal current layer. Electron energization is inferred from light emission near the antenna.

The experiments are performed in an unmagnetized afterglow plasma produced by a pulsed dc discharge shown schematically in Fig. 1. An insulated magnetic loop antenna (15 cm diam, 4 turns) is inserted into the uniform plasma center and energized by a damped oscillatory current ($I_{\max} \simeq 150$ A, frequency $\omega/2\pi \simeq 200$ kHz $\ll \omega_p/2\pi \simeq 3$ GHz). The magnetic field inside the plasma is measured with a three-component magnetic probe movable along three orthogonal axes. The space-time dependence of the field $\mathbf{B}(\mathbf{r}, t)$ is obtained from repeated, highly reproducible discharges. Measurements are also done in vacuum so as to distinguish the fields produced by antenna and plasma currents.

A large amplitude ac current ($I_{\max} \simeq 150$ A) is produced by switching a charged capacitor ($C = 0.1$ μF, 1000 V) into the antenna ($L = 5.7$ μH) with little circuit resistance ($R = 0.58$ Ω), producing a weakly damped ringing waveform ($f \simeq 200$ kHz). In plasma, the damping is enhanced ($\Delta R = 0.62$ Ω) and power is deposited into the plasma, $I^2_{\text{peak}}\Delta R/2 \simeq 7$ kW. Since this power cannot be radiated ($\omega \ll \omega_p$), it must be dissipated, and both location and dissipation processes are of interest. We first address the field topologies.

The rising magnetic field of the antenna in the first quarter cycle of the coil current oscillation induces plasma currents that oppose the field penetration. The reverse happens in the second quarter cycle: when the antenna field decreases, the induced plasma currents try to maintain the embedded magnetic field. After half a cycle, the coil current vanishes, but a significant dipolar magnetic field remains embedded in the plasma.

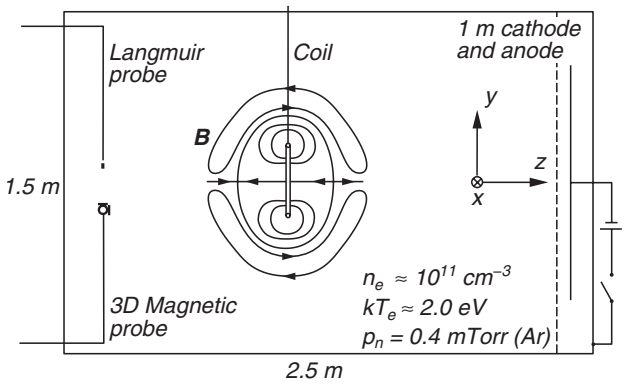

FIG. 1. Schematic of the experimental setup with typical parameters and schematic field lines of a field-reversed configuration.

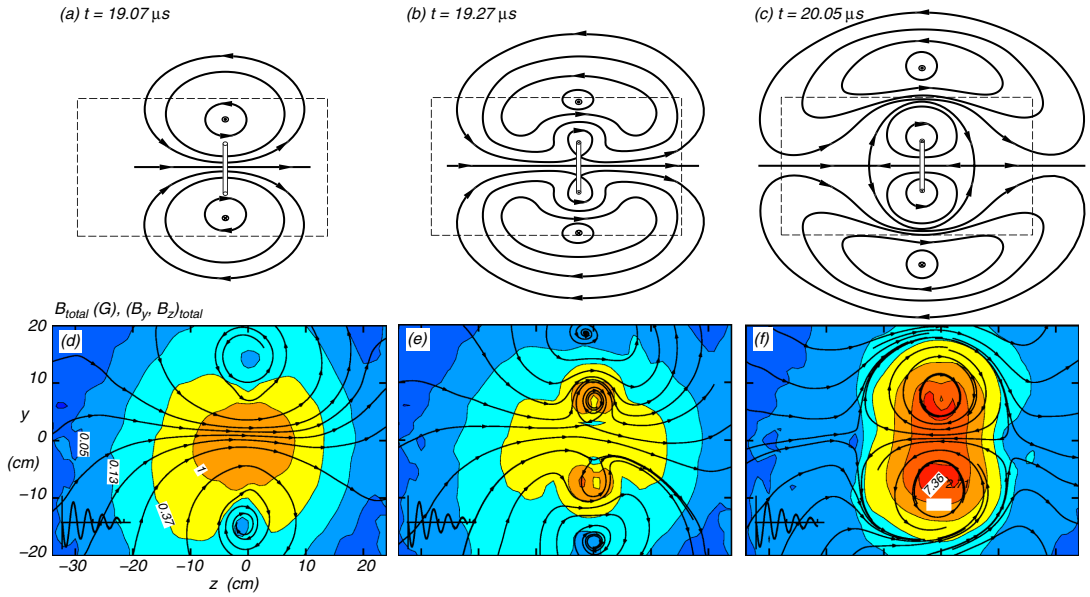

FIG. 2 (color online). Schematic field lines (a)–(c) and measured magnetic field properties [(d)–(f), stream lines, magnitude contours] in the y-z plane ($x = 0$) during coil current reversals, showing the formation of a field-reversed configuration.

In the second half cycle, a reverse antenna field rises and penetrates into the remnant field, thereby creating the field topology of an FRC. This process repeats at every subsequent current reversal. Figure 2 explains the change in field topology schematically, supported by observations. At the zero crossing of the coil current [Figs. 2(a) and 2(d)], a dipole field is maintained by a toroidal electron current. Just after coil current reversal [Figs. 2(b) and 2(e)], an X-type toroidal null line develops inside the coil. With increasing coil current, the null line moves toward the axis, forms a single degenerate null point which splits into two regular 3D null points forming an FRC [Figs. 2(c) and 2(f)]. The FRC expands axially with further increase in coil current, and the O-type toroidal null line, associated with the plasma current, expands radially away from the coil. If the mode was not evanescent, it would produce the field of a Hertzian magnetic dipole or nested FRCs.

In addition to the poloidal field components (B_y, B_z), there is also a toroidal field component B_θ, resulting in magnetic helicity. Figure 3(a) shows that, for $I_{\text{coil}} = 0$, the out-of-plane field component B_x exhibits a quadrupolelike pattern, resulting from a cut through two opposing toroidal fields. It is produced by the toroidal electron drift which convects the frozen-in poloidal field lines [Fig. 3(c)] out of the y-z plane. From the measured poloidal flux, $\Phi = \int B_z 2\pi r dr$, one finds the toroidal vector potential, $A_\theta = \Phi/2\pi r$, which is displayed in Fig. 3(b). The magnetic helicity density, shown in Fig. 3(d), is positive in the left hemisphere and negative for $z > 0$ and vanishes when integrated over all space. The sign is the same for each half cycle. These are the properties of whistler modes propagating along or against a background magnetic field [14], which, in the present case, is produced by plasma currents. Helicity is not created during diffusive field penetration.

Next we show that the magnetic bubble expands nonlinearly with field strength. While the free-space antenna field distribution is independent of amplitude, the induced field produced by plasma currents has an amplitude depen-

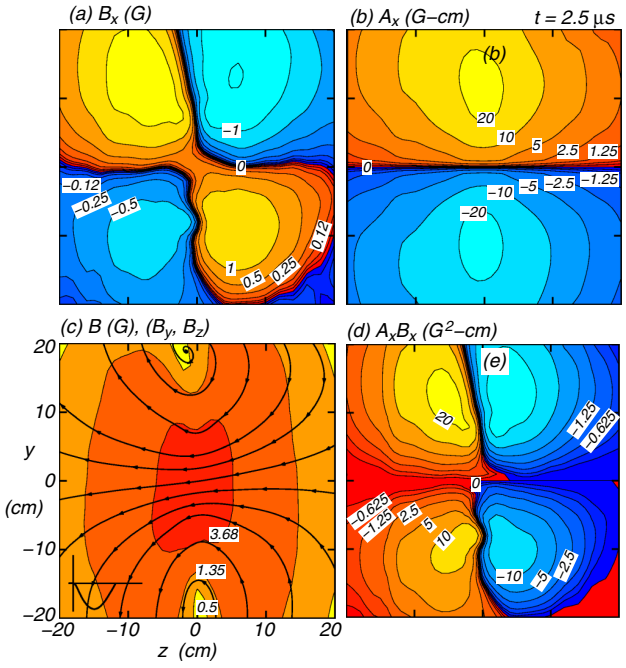

FIG. 3 (color online). Helicity creation in a field-free plasma. (a) Out-of-plane magnetic field component $B_x(x = 0, y, z)$. (b) Vector potential A_x. (c) Total magnetic field as unit vectors and contours of field strength. (d) Magnetic helicity density A_xB_x. Inset in (c) shows coil current waveform at the time of the displays.

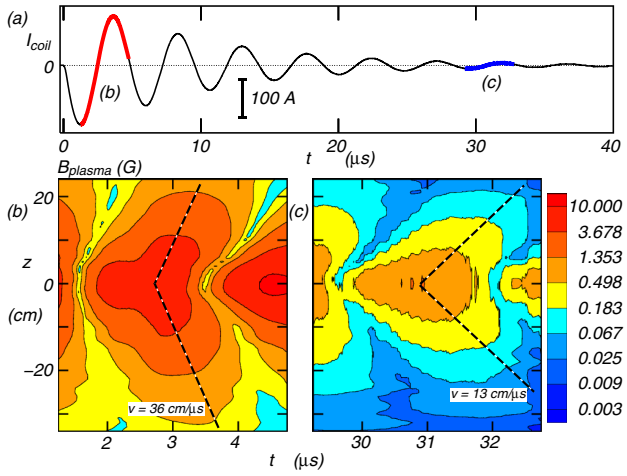

FIG. 4 (color online). (a) Coil current waveform and comparison of the field penetration speed at (b) large and (c) small field strengths. Contour plot of $B_{\mathrm{plasma}}(0, 0, z, t)$ shows faster propagation, hence further penetration, with increasing amplitude. The contour spacings correspond to an e-folding amplitude change.

dence. Figure 4 shows contour plots of $B_{\mathrm{plasma}}(0, 0, z, t)$ together with the coil current waveform. The penetration velocity increases with amplitude; hence, for a given rf period the larger fields propagate farther into the plasma. This is explained by the magnetization of the electrons, which occurs when the Larmor radius becomes smaller than either the collisional mean free path or the gradient scale length of the field. For the present parameters ($n \simeq 2 \times 10^{11}$ cm^{-3}, $kT_e \simeq 2$ eV), the mean free path due to the dominant Coulomb collisions is $v_e/\nu_{ei} \simeq 21$ cm, which equals an electron Larmor radius at $B \simeq 0.23$ G. At large, but not small, coil currents, the electrons are magnetized over most of the measurement volume. This allows the field to penetrate in the whistler mode since the applied frequency (200 kHz) is below the cyclotron frequency when $B > 0.07$ G. The whistler group velocity increases with magnetic field strength [$v_{\mathrm{group}} \simeq 2(c/\omega_p)(\omega\omega_c)^{1/2} \simeq 36$ cm/μs at 10 G]. At very small amplitudes the scale length approaches the collisional skin depth $(2/\omega\mu_0\sigma)^{1/2} \simeq 3$ cm.

Electron currents and electric fields are derived from magnetic fields, which have been measured both in plasma and in vacuum so as to distinguish antenna from plasma fields. Of particular interest are times when coil current and electric field reverse sign, as shown in Fig. 5. When the coil current reverses the inductive electric field, $E_\theta = -\partial A_\theta/\partial t$ drives a toroidal plasma current, which produces a significant poloidal magnetic field ($B_{z,\mathrm{max}} \simeq 10$ G). Just after coil current reversal [Figs. 5(a)–5(d)], the total magnetic field near the coil exhibits an FRC topology but the plasma field and current remain relatively unchanged. When the coil current passes through a maximum (or minimum), the inductive electric field $E_\theta \propto \partial I_{\mathrm{coil}}/\partial t$ reverses sign. As shown in Figs. 5(e)–5(h), the electric field reversal starts at the coil, drives a reverse toroidal current to shield the coil field, and creates an FRC topology in the *plasma* field but not in the total field, which is dominated by the large coil current. As the coil current decreases, the reversed electric field and current expand and, when $I_{\mathrm{coil}} = 0$, assume profiles as in Figs. 5(c) and 5(d) except with reversed signs. There is also a strong space charge field, $\mathbf{E} = \mathbf{J} \times \mathbf{B}/ne$, in addition to the inductive electric field, to produce the toroidal electron Hall current.

Electric and magnetic fields yield the Poynting vector, $\mathbf{S} = \mathbf{E} \times \mathbf{H}$. When $|I|_{\mathrm{coil}}$ grows from zero to $|I|_{\mathrm{coil,max}}$, the energy flows out of the FRC separatrix

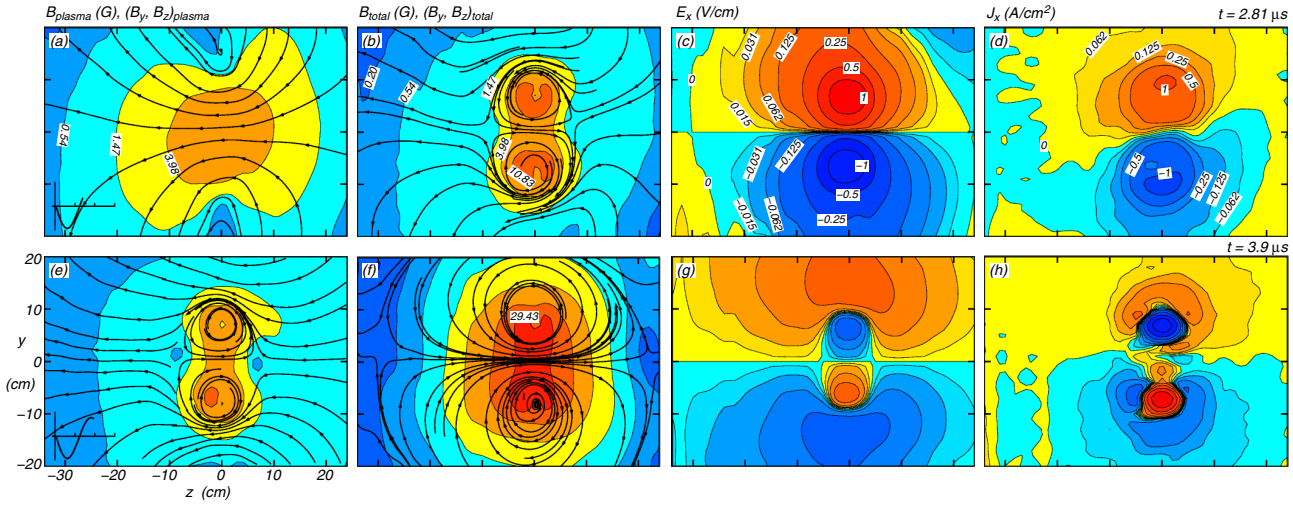

FIG. 5 (color online). Magnetic fields, electric fields, and plasma currents at two characteristic times. When the coil current reverses sign (a)–(d), a strong dipolar plasma field (a) is produced by toroidal currents (d) driven by a toroidal electric field (c) while the total magnetic field (b) has an FRC topology since the antenna field reverses. When the coil current decays from $|I|_{\mathrm{max}}$, the electric field (g) reverses sign, creating two opposing coaxial plasma currents (h), an FRC topology in the plasma field (e), while the total field (f) remains dipolar since dominated by I_{coil}.

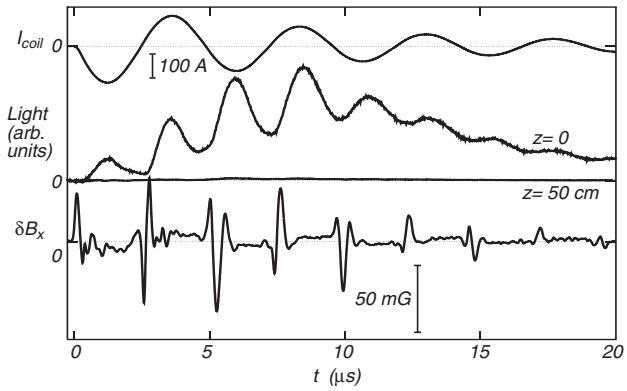

FIG. 6. Waveforms of the coil current (top line), the light emission, observed radially at and far from the coil (middle line), and high-frequency magnetic oscillations, $\delta B_x(z = 0, t)$ (bottom line).

[Figs. 5(b) and 5(c)]. When $|I|_{\text{coil}}$ decreases from $|I|_{\text{coil,max}}$ to zero, the Poynting vector points toward the coil where the electric field has reversed, but in regions of the original electric field $\mathbf{S}$ points away from the coil [Figs. 5(g) and 5(h)]. The Poynting vector associated with the plasma fields, $\mathbf{S} = \mathbf{E} \times \mathbf{H}_{\text{plasma}}$, always transports energy radially and axially outward, while $\mathbf{E} \times \mathbf{H}_{\text{coil}}$ points both toward and away from the loop. Hall electric fields produce rotational Poynting vectors and no radial energy transport.

Finally, we have also observed electron heating and nonlinear magnetic oscillations. As shown in Fig. 6, a peak in light emission is observed at each current extremum at the antenna location ($z = 0$), but not at a distance of $z = 50$ cm. Light excitation from electron-neutral collisions in Argon requires electron energies >10 eV which are not present in the afterglow plasma. Each light pulse has the same rise and fall time; hence, electrons must lose their energy as fast as they gain it. The light also peaks when the inductive electric field vanishes and the magnetic field maximizes. These features indicate that the electrons gain and loose perpendicular kinetic energy by magnetic compression, $mv_\perp^2/2 = \mu B$, where μ is the adiabatic invariant. Collisions degrade the adiabaticity and cause true heating which is manifested by the slowly rising and falling background light on which the oscillations ride. Electron heating causes the dissipation of the applied fields.

Careful inspection of the magnetic field signals reveals transient oscillations at each coil current zero crossings (Fig. 6). The oscillations are extracted by smoothing the original waveform and displaying the difference. The oscillations are a nonlinear phenomenon which occur only at large coil currents [15]. They peak when the light has a minimum and hence are not created by fast electrons. Spatially the oscillations originate near the antenna when the O-type toroidal null line forms and propagates radially outward. In the presence of an FRC, the waves propagate on diverging field lines both axially and radially away from the antenna. Propagation is limited to a volume where the electrons are magnetized. The nonuniform and time-varying background magnetic field does allow a simple mode identification in terms of plane waves, but since the only mode in the present parameter regime is the whistler, it is believed that the magnetic oscillations are small-amplitude whistlers triggered by rapid current formations associated with the topology changes.

In summary, we have shown that a strong oscillatory magnetic field applied to an initially unmagnetized plasma magnetizes the electrons which allows the field to penetrate nonlinearly in the whistler mode. FRC field topologies arise with local helicity density characteristic of whistler modes. Electrons are energized by adiabatic compression. Transient magnetic oscillations are created near magnetic null lines and excite whistler modes in a nonuniform magnetic structure. These findings are of intrinsic interest in nonlinear field-plasma interactions and in applications such as active magnetic bubbles in space plasmas [16] or inductively coupled rf plasma sources.

The authors gratefully acknowledge support from the NSF/DOE Partnership Grant ER54905.

*stenzel@physics.ucla.edu

[1] H. Shindo, D. Kudo, and S. Fujii, Jpn. J. Appl. Phys. **41**, L956 (2002).
[2] A. Fruchtman and L. I. Rudakov, Phys. Rev. Lett. **69**, 2070 (1992).
[3] V. S. Sonwalkar, U. S. Inan, T. F. Bell, R. A. Helliwell, O. A. Molchanov, and J. L. Green, J. Geophys. Res. **99**, 6173 (1994).
[4] F. F. Chen, Phys. Plasmas **8**, 3008 (2001).
[5] E. S. Weibel, Phys. Fluids **10**, 741 (1967).
[6] K. C. Shaing, Phys. Plasmas **3**, 3300 (1996).
[7] V. A. Godyak and V. I. Kolobov, Phys. Rev. Lett. **79**, 4589 (1997).
[8] K. Minami, K. P. Singh, M. Masuda, and K. Ishii, Phys. Rev. Lett. **33**, 740 (1974).
[9] J. M. Urrutia and R. L. Stenzel, Phys. Rev. Lett. **67**, 1867 (1991).
[10] V. Godyak, B. Alexandovich, R. Piejak, and A. Smolyakov, Plasma Sources Sci. Technol. **9**, 541 (2000).
[11] K. Chukbar, A. A. Ivanov, Jr., and V. V. Smirnov, J. Plasma Phys. **60**, 761 (1998).
[12] A. S. Kingsep, K. V. Chukbar, and V. V. Yan'kov, in *Reviews of Plasma Physics*, edited by B. B. Kadomtsev (Consultants Bureau, New York, 1990), Vol. 16, p. 243.
[13] M. Tuszewski, Nucl. Fusion **28**, 2033 (1988).
[14] C. L. Rousculp, R. L. Stenzel, and J. M. Urrutia, Phys. Plasmas **2**, 4083 (1995).
[15] J. M. Urrutia, R. L. Stenzel, and K. D. Strohmaier, Phys. Plasmas **15**, 062109 (2008).
[16] A. Biancalani, F. Ceccherini, and F. Pegoraro, Plasma Sources Sci. Technol. **17**, 024006 (2008).